

Discovery of a metal-poor, luminous post-AGB star that failed the third dredge-up.

D. Kamath

and

H. Van Winckel

Instituut voor Sterrenkunde, K.U.Leuven, Celestijnenlaan 200D bus 2401, B-3001 Leuven,
Belgium

P. R. Wood

and

M. Asplund

Research School of Astronomy and Astrophysics, Australian National University, Canberra
ACT 2611, Australia

A.I. Karakas

Research School of Astronomy and Astrophysics, Australian National University, Canberra
ACT 2611, Australia

Monash Centre for Astrophysics, School of Physics and Astronomy, Monash University,
VIC 3800, Australia

J. C. Lattanzio

Monash Centre for Astrophysics, School of Physics and Astronomy, Monash University,
VIC 3800, Australia

Received _____; accepted _____

ABSTRACT

Post-asymptotic giant branch (post-AGB) stars are known to be chemically diverse. In this paper we present the first observational evidence of a star that has failed the third dredge-up (TDU). J005252.87-722842.9 is a A-type ($T_{\text{eff}} = 8250 \pm 250\text{K}$) luminous ($8200 \pm 700 L_{\odot}$), metal-poor ($[\text{Fe}/\text{H}] = -1.18 \pm 0.10$), low-mass ($M_{\text{initial}} \approx 1.5 - 2.0 M_{\odot}$) post-AGB star in the Small Magellanic Cloud. Through a systematic abundance study, using high-resolution optical spectra from UVES, we found that this likely post-AGB object shows an intriguing photospheric composition with no confirmed carbon-enhancement (upper limit of $[\text{C}/\text{Fe}] < 0.50$) nor enrichment of s -process elements. We derived an oxygen abundance of $[\text{O}/\text{Fe}] = 0.29 \pm 0.1$. For Fe and O, we took into account the effects of non-local thermodynamic equilibrium (NLTE). We could not derive an upper limit for the nitrogen abundance as there are no useful nitrogen lines within our spectral coverage. The chemical pattern displayed by this object has not been observed in single or binary post-AGBs. Based on its derived stellar parameters and inferred evolutionary state, single star nucleosynthesis models predict that this star should have undergone TDU episodes while on the AGB and be carbon-enriched. However, our observations are in contrast with these predictions. We identify two possible Galactic analogues which are likely to be post-AGB stars, but the lack of accurate distances (hence luminosities) to these objects does not allow us to confirm their post-AGB status. If they have low luminosities then they are likely to be dusty post-RGB stars. The discovery of J005252.87-722842.9 reveals a new stellar evolutionary channel whereby a star evolves without any third dredge-up episodes.

Subject headings: (galaxies:) Magellanic Clouds, methods: observational, stars:

abundances, stars: AGB and post-AGB, stars: chemically peculiar, stars: evolution

1. Introduction

Post-asymptotic giant branch (post-AGB) stars are low- to intermediate-mass stars that have evolved off the AGB because a strong dusty mass loss removed most of the stellar envelope. This mass loss occurs either by binary interaction or, for single stars, by a phase of very high mass-loss called the superwind (e.g., Nie et al. 2012, and references therein). Their atmospheres contain signatures of the chemical enrichment from internal nucleosynthesis that has occurred prior to and during their entire AGB lifetime. For single stars, during the thermally pulsing AGB (TP-AGB) phase, the photospheric abundance of the object can be altered in two ways. Firstly, via third dredge-up (TDU) episodes that can occur after a thermal pulse. These are responsible for enriching the stellar photosphere with products of internal nucleosynthesis such as carbon (C), nitrogen (N), oxygen (O) and heavy elements produced by the slow neutron capture process (*s*-process, see Karakas & Lattanzio 2014, for a review). They can also convert stars into carbon-rich (C-rich) stars with a C/O ratio greater than unity (Herwig 2005). Secondly, via hot bottom burning (HBB), which is thought to be only active in stars of initial mass greater than $4 - 5 M_{\odot}$. HBB prevents the formation of carbon-rich photospheres by burning ^{12}C into ^{14}N (Boothroyd et al. 1993; Lattanzio 1992; Lattanzio et al. 1996; Karakas & Lattanzio 2007; Ventura et al. 2015). We note that stellar evolutionary sequences and nucleosynthesis models are metallicity and mass dependant and are subjected to many uncertainties (see Karakas & Lattanzio 2014, for a review).

During the post-AGB phase, the warm stellar photosphere makes it possible to quantify photospheric abundances for a very wide range of elements from CNO up to some of the heaviest *s*-process elements well beyond the Ba peak (Reyniers & Van Winckel 2003), that are brought to the stellar surface during the AGB phase (Busso et al. 2001; Cristallo et al. 2011; Fishlock et al. 2014). Therefore, post-AGB objects can provide direct and stringent

constraints on the parameters governing stellar evolution and nucleosynthesis, especially during the chemically-rich AGB phase.

Post-AGB stars are surrounded by the relic of a heavy mass-loss episode. Therefore, they have a dusty circumstellar environment which is characterised by a large mid-infrared (mid-IR) excess. This has allowed for the identification and study of post-AGB stars in the Galaxy and in the Magellanic Clouds.

Extensive studies using Galactic post-AGB objects have also shown that the majority of the optically visible post-AGB stars can be classified into two groups based on their spectral energy distributions (SEDs, see Van Winckel 2003, for a review). The first group of objects, referred to as shell-type sources, display a double peaked SED. The peak at shorter wavelengths is due to emission from the stellar photosphere and the peak at longer wavelengths is due to circumstellar dust which usually peaks at wavelengths greater than $10\mu\text{m}$. This has been illustrated from radiative transfer models of a well known expanding shell source HD161796, where the peak of the dust SED is at around $30\mu\text{m}$ (Min et al. 2013). This type of SED is most likely characteristic of single post-AGB stars surrounded by an optically thin expanding circumstellar envelope that is the remnant AGB mass-loss. The shell continues to move outwards, gradually exposing the central star, resulting in a double-peaked SED. These objects mostly contain the photospheric chemistry that is representative of single stars. The second group of objects display SEDs with a clear near-infrared ($\lambda < 10\mu\text{m}$) excess indicating that circumstellar dust must be close to the central star, near the sublimation temperature. It is now well established that this feature in the SED indicates the presence of a stable compact circumbinary disc (see Van Winckel 2003, for a review). The commonly accepted evolutionary scenario that results in the formation of a circumbinary disc is that during the star’s ascent up the AGB, it suffers a strong interaction with a companion (likely to be an unevolved main-sequence star). The

AGB star fills its Roche lobe and stable mass transfer ensues which results in the formation of a circumbinary disc. What we observe is then a F- or G-type post-AGB supergiant in a binary system, surrounded by a circumbinary dusty disc. Therefore dusty discs are considered to be characteristic of binary post-AGB stars. These sources are referred to as disc-sources (e.g., de Ruyter et al. 2006; Deroo et al. 2007; Gielen et al. 2011; Hillen et al. 2013). The rotation of the disc has been resolved with the ALMA array (Bujarrabal et al. 2013b, 2015) in two objects and our survey using single dish observations confirms that disc rotation is indeed widespread (Bujarrabal et al. 2013a) .

Galactic post-AGB objects not only show a diversity in SED characteristics but are also chemically more diverse than anticipated. Kwok et al. (1989) found an emission feature at 21 microns that was only observed in C-rich post-AGB stars (thereafter known as 21 micron sources), with a varying strength but constant line profile (Volk et al. 1999). Klochko (1995) discovered strong *s*-process lines in the Galactic 21 micron source HD56126. Subsequently, as expected for these objects, many studies (e.g., Van Winckel & Reyniers 2000; Reddy et al. 2002; Reyniers & Van Winckel 2003; Reyniers et al. 2007) revealed *s*-process overabundances in objects with clear C-rich dust. These objects are likely to have evolved via the single star evolutionary scenario. It was also found that post-AGB objects that have O-rich dust chemistry are not *s*-process enriched (Van Winckel 2003). An example is the dusty high-latitude A-F supergiants, which are metal poor, C-enhanced, more strongly N-enhanced, and not enhanced or deficient in *s*-process elements (Luck et al. 1990). Furthermore, many non *s*-process enriched objects show a characteristic chemical pattern of ‘depletion’ of refractory elements in their photosphere whereby elements with a high dust-condensation temperature (such as Fe, Ti, Ca and Cr) are systematically under-abundant (Van Winckel et al. 1998; Giridhar et al. 2000; Maas et al. 2005; Deroo et al. 2005; Gezer et al. 2015). The process to acquire this chemical anomaly is not completely understood, but it is believed that radiation pressure on the circumstellar dust

grains results in a chemical fractionation of dust and gas in the circumstellar environment. The cleaned gas (with C, N, O, S and Zn) is then re-accreted onto the stellar surface making the photosphere devoid of refractory elements (see review by Van Winckel 2003). As a result of this process, the stars display a peculiar photospheric composition similar to the interstellar gas. Waters et al. (1992) proposed that the most likely circumstance for the process to occur is when the dust is trapped in a circumstellar disc. In almost all depleted post-AGB objects, there is observational evidence that a stable circumbinary disc is present (de Ruyter et al. 2006; Gezer et al. 2015) which seems to be a prerequisite to obtain photospheric depletion patterns. Therefore it is likely that these objects follow the binary evolution scenario mentioned above. Furthermore, the circumstellar dust in the disc is O-rich (Gielen et al. 2008) implying that formation of the disc occurred when the object was still an M-type AGB star. In some disc sources double chemistry is detected in which the C-rich component is mainly limited to polycyclic aromatic hydrocarbon (PAH) emission (Gielen et al. 2009). This does not necessarily mean that the central object is a carbon star, as PAH emission is also found in environments where dissociation of CO can liberate C atoms (Geballe et al. 1989; Witt et al. 2009; Guzmán-Ramírez et al. 2011).

Though the Galactic sample is observationally well studied and has revealed important chemical and morphological characteristics of post-AGB stars, the so-far poorly constrained distances and hence initial masses and luminosities, pose a severe limitation on our ability to fully exploit this assorted group of objects. The recent first Gaia data release, (Gaia DR1, Gaia Collaboration et al. 2016), has provided parallaxes to a small sample of known Galactic post-AGB stars however the errors in their parallaxes are too large to be able to accurately determine their distances. Unknown distances (and hence luminosities and initial masses) hamper the interpretation of the diversity in the photospheric chemistry as well as the morphology of these objects as a function of luminosity and mass.

In our recent studies, we exploited the release of the infrared Large Magellanic Cloud (LMC) and Small Magellanic Cloud (SMC) SAGE-Spitzer surveys of Meixner et al. (2006) and Bolatto et al. (2007) to identify optically bright evolved stars with infrared colours indicative of a past history of heavy dusty mass loss in the LMC (van Aarle et al. 2011; Kamath et al. 2015) and SMC (Kamath et al. 2014). Realising the importance of the spectral characterisation of the central objects to confirm their post-AGB nature, we performed a low-resolution optical spectral survey with the AAOmega multi-fibre spectrograph with a 2 degree field of view (Lewis et al. 2002), mounted on the Anglo Australian 3.9m telescope. Our detailed spectral analysis resulted in a clean and extensive census of well characterised post-AGB stars with spectroscopically determined stellar parameters T_{eff} , $\log g$, $[\text{Fe}/\text{H}]$ and $E(B - V)$ spanning a wide range of luminosities in the LMC (Kamath et al. 2015) and SMC (Kamath et al. 2014). Additionally, our survey also resulted in the discovery of dusty post-red giant branch stars (post-RGB) stars, which display similar stellar parameters and SED characteristics as post-AGB stars but have lower luminosities ($L/L_{\odot} \leq 2500$). These objects are believed to have evolved off the RGB via binary interaction (see Kamath et al. 2016).

By virtue of their spectral types, favourable bolometric corrections and especially their constrained distances, the Magellanic Cloud (MC) post-AGB stars offer unprecedented tests for AGB theoretical structure and enrichment models of low- and intermediate-mass stars. The photospheric chemistry of a small fraction of these post-AGB stars in the MCs have been studied in detail until now. The first chemical abundance studies, carried out by Reyniers et al. (2007) and Gielen et al. (2009), showed a depletion pattern. As expected, all these objects had dusty circumstellar discs, which, together with their depleted photospheric chemistry points to their binary nature. Our recent high-resolution chemical abundance studies, also resulted in the discovery of the most *s*-process enriched post-AGB star in the SMC (De Smedt et al. 2012). This object is likely to be a single, luminous ($L/L_{\odot} \approx 7000$),

C-rich, 21 micron source with shell-type SED. In our subsequent studies, we found more *s*-process enriched objects with shell-type SEDs (van Aarle et al. 2013; De Smedt et al. 2015). The MC post-AGB objects therefore also follow the same chemical diversity and morphology as that of the Galactic objects.

In this paper we present a detailed chemical abundance study of a chemically peculiar post-AGB star, J005252.87-722842.9 (hereafter referred to as J005252), that resides in the SMC. In the following sections of the paper we present our detailed spectral analysis (determination of stellar parameters as well as the abundance analysis) of J005252 along with an interpretation of our results. We also present the likely Galactic analogues of J005252. Finally, we conclude with a summary of our study and its implications for stellar evolution.

2. Data and Observations

2.1. Photometry

J005252 was first identified as a post-AGB candidate in our extensive low-resolution spectroscopic survey (Kamath et al. 2014). The photometry covering the optical, near-IR and mid-IR bands are presented in Kamath et al. (2014). Figure 1 shows the SED for J005252. The SED is constructed using the broadband photometry. The full procedure that we used to correct for foreground extinction (which takes into account the extinction produced by the interstellar dust in our Galaxy, along the line of sight of the SMC and from the SMC itself), is mentioned in Kamath et al. (2014, 2015). In brief, we use the extinction law of Cardelli et al. (1989) with a mean reddening, for the combined SMC and Galactic components, of $E(B-V) = 0.12$ (Keller & Wood 2006).

Based on the visual inspection of the dust excess in the SED of this object (see

Figure 1), it appears to be a shell-type source with an expanding dusty circumstellar shell. In Figure 1, we show the SED of a post-AGB star (J050632.10-714229.8) with a shell-type SED (van Aarle et al. 2013) and a post-AGB star (J052832.60-690440.6) with a disc-type SED (Kamath et al. 2015). From this comparison, it can be clearly seen that the SED of J005252 is shell-type. The observed luminosity of this object (L_{obs}) is $8000 L_{\odot}$ (see Kamath et al. 2014), and was obtained by integrating the SED that is defined by the photometry corrected for foreground extinction while applying a distance modulus for the SMC of 18.93 (Keller & Wood 2006). The integration was not extended beyond the available wavelength points in the flux distribution. Therefore, the estimated observed luminosity is a lower limit. The circumstellar extinction was not corrected for because it was assumed that all radiation absorbed by the circumstellar matter was re-radiated at a longer mid-IR wavelength still within the wavelength range of the observed SED. In Section 3.2 we estimate the total line-of-sight extinction towards J005252, which is the sum of the Galactic, SMC and circumstellar reddening. Using this total extinction we derive the photospheric luminosity by integrating under the full model atmosphere appropriate for J005252 (see Section 3.2) which provides a more accurate luminosity of the central star of this object than the observed luminosity (L_{obs}/L_{\odot}).

2.2. Spectroscopic observations and data reduction

We obtained high-resolution optical spectra using the UVES echelle spectrograph (Dekker et al. 2000), mounted on the 8m UT2 Kueyen Telescope of the VLT array at the Paranal Observatory of ESO in Chile. We used the dichroic beam-splitter which resulted in a wavelength coverage in the blue arm from approximately 3280 to 4530 Å and in the red arm for the lower and upper part of the mosaic CCD chip from approximately 4780 to 5770 Å and from 5800 to 6810 Å, respectively. We chose a slit width of 1 arcsecond to

obtain a good compromise between spectral resolution and slit-loss minimisation. The details of the object along with its coordinates are listed in Table 1.

The UVES raw data were reduced using the UVES pipeline (version 5.3.0) in the Reflex environment of ESO. The reduction process included the standard procedures for echelle data reduction: background correction, extraction of the spectral orders with cosmic-clipping, flat-fielding and wavelength calibration. For spectra reduced within the Reflex environment, the standard reduction parameters of the UVES pipeline were used as these resulted in the best signal-to-noise (S/N). Once reduced, the weighted mean spectra were created for the three different wavelength regions. Each sub-spectrum was then normalised individually by fitting a fifth order polynomial through interactively defined continuum points. Finally, the subspectra were merged into one large spectrum, which is used for the spectral analysis. During merging, the mean flux was calculated for the overlapping spectral regions of the subspectra. The final spectrum has a mean S/N of 90 in the red part and a S/N ranging from 25 to 45 in the blue (above 4000 Å). In Figure 2 we show samples of our available spectra to illustrate the quality of our obtained data.

In Kamath et al. (2014), we established the SMC membership of J005252 using low-resolution spectra. In this study, we used our optical high-resolution spectra and confirmed the SMC membership of J005252. Using the Fourier cross-correlation technique we derived its heliocentric radial velocity to be $149 \pm 1 \text{ km s}^{-1}$. We note that for the cross-correlation we used the neutral oxygen lines, the O I triplet, at 6155.97, 6156.78 and 6158.19 Å. The estimated heliocentric radial velocity agrees well with the velocity ($\approx 160 \text{ km s}^{-1}$) expected for stars in the SMC (De Propris et al. 2010).

3. Spectral analysis

To study the photospheric composition of J005252, we performed a systematic spectral analysis. We first estimated accurate atmospheric parameters for this object and then we carried out a detailed abundance study. The spectral analysis was performed using PyMoog, our own Python wrapper around the local thermal equilibrium (LTE) abundance calculation routine MOOG (Snedden 1973). For the spectral analysis we used the LTE Kurucz-Castelli atmosphere models (Castelli & Kurucz 2003) and the spectral lines were identified using linelists, ranging from 3000 to 11000 Å, from the VALD database (Kupka et al. 1999) combined with the linelist of ‘Instituut voor Sterrenkunde’ (Van Winckel & Reyniers 2000). Full details of PyMoog and our spectral analysis are presented in De Smedt et al. (2015, and references therein). In the following subsections we briefly describe our spectral analysis and the obtained results.

3.1. Atmospheric parameter determination

The atmospheric parameters of J005252 were determined using both Fe I and Fe II lines combined with standard spectroscopic methods. We determined the effective temperature (T_{eff}) by requiring the iron abundance to be independent of lower excitation potential. Since the low-resolution spectroscopic analysis of J005252 carried out in Kamath et al. (2014) as well as the high-resolution high S/N spectra (available as online supporting information) revealed the object to be of spectral-type A, we chose the Fe II lines (since at these temperatures most of the Fe is present as Fe II than Fe I) for the temperature determination. We determined the surface gravity ($\log g$) by imposing ionisation equilibrium between the individual Fe I and Fe II abundances. The microturbulent velocity (ξ_t) was determined by requiring the iron abundance to be independent of the reduced equivalent width (EW/λ). Similar to the effective temperature determination, we chose Fe II lines for

the microturbulent velocity determination.

We decreased the parameter steps of the Kurucz atmosphere models using linear interpolation to calculate atmospheric models which lie within the parameter steps. We did not do any extrapolation. We chose T_{eff} steps of 125 K, $\log g$ steps of 0.25 dex and ξ_t steps of 0.25 km s^{-1} . The atmospheric parameter and radial velocity estimates for J005252 are listed in Table 2. The estimated abundances of $[\text{Fe I}/\text{H}]$ and $[\text{Fe II}/\text{H}]$ differ by 0.10 dex (see Table 2). For warm, low-gravity stars such as J005252, departures from LTE can be expected to be significant for many, if not most, elements and transitions. Such non-LTE (NLTE) effects on the level populations are largely driven by the intense radiation field at shorter wavelengths and are not compensated by thermalising collisions in the low density atmosphere of J005252. Neutral, relatively low-ionisation minority species such as Fe I are affected by over-ionisation which makes the lines weaker while the overall population of Fe II, being the dominant ionisation stage, is well approximated by the Saha distribution (e.g., Asplund 2005). This difference makes it important to take NLTE effects into account for the surface gravity determination in particular. For the purpose we have made use of the extensive 1D non-LTE calculations for Fe by Amarsi et al. (2016); the employed Fe model atom is described further in Lind et al (in preparation) but we note that we make use of new, realistic quantum mechanical-based cross-sections for inelastic collisions between Fe and H (Barklem et al., in preparation). For J005252 we find typical non-LTE effects for Fe I of 0.18 dex while Fe II is essentially unaffected (≤ 0.01 dex). We note that while absolute abundances can be sensitive to the adopted model atmospheres, the NLTE abundance corrections are much less so, and therefore consider the inconsistency between the Kurucz-Castelli model atmospheres used for the LTE abundance analysis and the MARCS (Gustafsson et al. 2008) models for the NLTE calculations to be of secondary importance compared with other uncertainties in the observations and analysis. We assume the estimated $[\text{Fe II}/\text{H}]$ abundance of the object as its metallicity ($[\text{Fe}/\text{H}]$). We

find that this object is metal poor ($[\text{Fe}/\text{H}] = -1.18 \pm 0.10$) when compared to the mean metallicity ($[\text{Fe}/\text{H}] \approx -0.7$) of the young stars in the SMC (Luck et al. 1998). The indicated uncertainties of $[\text{Fe I}/\text{H}]$ and $[\text{Fe II}/\text{H}]$ are the total errors on the iron abundances which includes line-to-line scatter and the atmospheric parameter uncertainties (see De Smedt et al. 2015, for full details on the error estimation). In Table 2 we present a comparison of the estimated atmospheric parameters of J005252 from this study to those obtained using the low-resolution AAOmega optical spectra (Kamath et al. 2014). The values from the high-resolution (UVES) and low-resolution (AAOmega) spectral analysis are mostly in good agreement however discrepancies in, for e.g., the $[\text{Fe}/\text{H}]$ values, indicate the need for high-resolution spectra to get reliable stellar parameters and abundances.

3.2. Reddening, luminosity and initial mass estimates

A main characteristic feature of a post-AGB star is its mid-IR excess. This large mid-IR excess results in a significant reddening, which included both the foreground extinction (see Section 2.1) as well as the circumstellar reddening. Therefore, it is important that we estimate the total reddening for J005252. To do this we follow a similar method used in Kamath et al. (2014). We calculated the $E(B - V)$ by estimating the value of $E(B - V)$ that minimised the sum of the squared differences between the de-reddened observed and the intrinsic B , V , I and J magnitudes. We used the extinction law by Cardelli et al. (1989), with a $R_v = 3.1$. We note that we included the uncertainty of the model atmosphere parameters (such as T_{eff} and $\log g$) in our minimisation. At longer wavelengths, emission from dust can contribute to the observed magnitudes. We note that, it is possible that the circumstellar extinction law is different from the interstellar extinction law but we have not explored this possibility. We derived a small $E(B - V)$ value of 0.02 ± 0.02 . The derived $E(B - V)$ values were used to correct the observed magnitudes for extinction. Then the

BVIJ fluxes of the best-fit (derived from the spectral analysis) LTE Kurucz-Castelli model atmosphere (Castelli & Kurucz 2003) were normalised to the corrected *BVIJ* fluxes. We note that the uncertainty on the reddening was computed by determining the confidence intervals of the free parameters.

For post-AGB stars, the central star is surrounded by circumstellar dust that is not necessarily spherically symmetric. For such cases, the observed luminosity L_{obs} (obtained by integrating the flux under the observed SED, see Section 2.1) could either be over-estimated or under-estimated. For this reason it is essential to estimate the photospheric luminosity of the central star L_{ph} . We determined this luminosity by integrating the model atmosphere scaled to the dereddened data. We estimated a photospheric luminosity of $8200 \pm 700 L_{\odot}$. The uncertainty on the luminosity is dominated by the uncertainty of the total line-of-sight reddening, which impacts strongly on the luminosity determination.

In Table 2 we present the SED results of J005252. The newly constructed SED is shown in Figure 1.

The determined luminosity and reddening agrees well with the values obtained using the low-resolution spectra for this object (Kamath et al. 2014).

Using the derived T_{eff} , $[\text{Fe}/\text{H}]$, and luminosity (L_{ph}), we determined the current mass of J005252 to be $0.63 \pm 0.02 M_{\odot}$ using the luminosity-core mass relation for AGB stars (Wood & Zarro 1981, the relation between core mass and quiescent luminosity, equation (3)). We also determined the initial mass to be $1.5 M_{\odot}$ to $2.0 M_{\odot}$ using the initial-final-mass relation (corresponding to a $Z = 0.001$) of Vassiliadis & Wood (1994). Models by Fishlock et al. (2014) yields a mass of $\sim 0.64 - 0.65 M_{\odot}$ from the luminosity of a model corresponding to a star near the tip of the AGB with $Z = 0.001$ and an initial mass of $\sim 2 M_{\odot}$. The $Z = 0.001$ FRUITY models by Cristallo et al. (2015), the COLIBRI models by Marigo et al. (2013) and the models by Ventura et al. (2014) yield a luminosity-core mass relationship

that is consistent with Fishlock et al. (2014) at $2.0 M_{\odot}$.

We note that there are uncertainties in these estimates which arise from depend the models used and the assumptions made in the modeling. To complicate this further there is considerable degeneracy in the model predictions around this mass range. The core-mass luminosity relation may give us a core-mass but working backwards to get the initial mass suffers significantly from this degeneracy.

3.3. Establishing the post-AGB nature of J005252

Our surveys for post-AGB stars in the MCs (Kamath et al. 2014, 2015) revealed that other classes of objects, such as core-He burning (CHeB) stars and pre-main sequence (PMS) stars can appear similar to post-AGB stars based on either their luminosities or dust excesses.

CHeB stars (of $6 - 10 M_{\odot}$) have similar luminosities as J005252. However, the CHeB phase is not predicted to involve heavy mass loss and hence stars in this phase should not have significant circumstellar dust emission. This is contrary to the situation for J005252 where the object shows an excess already at 8 microns (of ~ 0.8 magnitudes) which continues up to $24 \mu\text{m}$ (see Figure 3). There is no information available on the mid-IR excess beyond $24 \mu\text{m}$. In the large sample of LMC Cepheids studied by Neilson et al. (2009), only $\sim 2\%$ have 8 micron excesses of this size or greater. Also, our object has a relatively low $\log g$ value. If this object was a CHeB star then it would be $\sim 8 - 12$ times more massive than a post-AGB star at the same luminosity (based on evolutionary tracks of Bertelli et al. 2008, for $Z=0.001$). They would therefore have a $\log g$ larger by ~ 1 dex. However this is not the case. Additionally, the metallicity of J005252 ($[\text{Fe}/\text{H}] = -1.18 \pm 0.10$) is lower than that expected from CHeB stars with $[\text{Fe}/\text{H}] = -0.7 \pm 0.15$ (based on a study of 12 cepheids

by Romaniello et al. 2005). Based on these arguments, J005252 is not likely to be a CHeB star.

Though PMS stars can have mid-IR excesses and luminosities similar to J005252, at a given luminosity, the mass of such a PMS star is about $\sim 15 - 20$ times that of the corresponding post-AGB star. This leads to a difference of ~ 1.2 in $\log g$ between a post-AGB star and a PMS star at a given luminosity (based on PMS evolutionary tracks of Tognelli et al. 2011). This gravity difference makes it more likely for J005252 to be a post-AGB star than a PMS star. Furthermore, the estimated metallicity (see Section 3.1) of J005252 is much lower ($Z \approx 0.001$) than the typical metallicity of young stars in the SMC ($Z \approx 0.004$). Hence if this object was to be a PMS star then it should have had the metallicity of the young stars in the SMC. This implies that our object is of lower mass (older) than PMS stars of the same luminosity.

Therefore, we conclude on balance that J005252 is likely a post-AGB star.

3.4. Abundance Analyses

We used the atmospheric parameters listed in Table 2 to calculate detailed abundances for J005252. We note that we analysed, in detail, the entire available spectral region (from 3300 to 4220 Å, 4790 to 5750 Å and 5840 to 6800 Å) but used only isolated non-blended lines for our abundance analysis. We did not use lines with EWs smaller than 5 mÅ because as they may be confused with spectral noise, nor larger than 150 mÅ, because these are saturated and formed in the upper layers of the photosphere where non-LTE effects are likely larger.

Based upon the ionisation potential of the corresponding ion, the element over iron ratios ($[X/Fe]$) were calculated using FeI or FeII. If the ionisation potential of an ion is

below the ionisation potential of Fe I, then the abundance of Fe I is used for calculating $[X/Fe]$. If the ionisation potential exceeds the ionisation potential of Fe I, Fe II was used for calculating $[X/Fe]$. The same principle was also used for calculating the total error of $[X/Fe]$. The errors were determined using the method described in Deroo et al. (2005). The uncertainties in the abundances, due to the atmospheric parameters, were calculated by determining the abundances of a certain ion for atmospheric models with $T_{\text{eff}} \pm 125 \text{ K}$, models with $\log g \pm 0.25 \text{ dex}$, and with microturbulent velocity $\xi_t \pm 0.2 \text{ km s}^{-1}$. The total uncertainties are therefore the quadratic sum of the uncertainties of the mean due to line-to-line scatter (σ_{121}), uncertainties due to atmospheric parameters and the Fe abundance uncertainty (σ_{Fe}), (see De Smedt et al. 2015, for further details on the error analysis).

The spectra are devoid of lines and the only elements that were identifiable from the spectra of J005252 are O ($Z=8$), Mg ($Z=12$), Si ($Z=14$), Sc ($Z=21$), Ti ($Z=22$), V ($Z=23$), Cr ($Z=24$), Fe ($Z=26$), and Ni ($Z=28$) and for these elements we determined their elemental abundances. The results of our abundance analysis are summarised in Table 4 and are also graphically presented in Figure 4. We take into account NLTE effects for Fe I (see Section 3.1) and for O I (see below). Unfortunately few NLTE studies of other elements for stellar parameters similar to J005252 have been performed to date and we therefore have to settle for the LTE abundances; we stress that there can be substantial systematic errors for individual elements as a result of this simplifying assumption. We encourage dedicated non-LTE calculations for key elements.

In table 3 we list all the spectral lines used in our abundance analysis. We note that the full table is available as online supporting information.

Our analyses reveals that J005252 has a rather intriguing abundance distribution. It is relatively metal poor (with $[Fe/H] = -1.18 \pm 0.10$) with $[O I/Fe] = 0.75 \pm 0.1$ and $[O I/H] = -0.89 \pm 0.06$. We take into account non-LTE effects for O I using the 1D non-LTE

computations by Amarsi et al. (2016). For the O I 6158 Å triplet, the non-LTE effects are very substantial in J005252: -0.41 dex.

J005252 shows no signs of C-enhancement. In our spectral coverage, the strongest usable lines of C are the neutral carbon (CI) lines at 5380.34 Å and 6587.62 Å. However, neither of the two lines were detected above the noise. Figure 5 shows the spectral regions that cover the 5380.34 Å and the 6587.62 Å CI lines. We used both lines to derive an upper limit for C which yielded a $[C/Fe]$ of 0.3, for an assumed EW of 5 mÅ. We were unable to estimate the abundance of N or provide an upper limit for the abundance as the strongest lines of N lie outside our spectral coverage.

J005252 also showed no signs of *s*-process enrichments. Stars that are *s*-process enriched show the presence of light *s*-elements (ls-elements) such as yttrium (Y, $Z=39$) and zirconium (Zr, $Z=40$), and heavy *s*-elements (hs-elements), such as barium (Ba, $Z=56$), lanthanum (La, $Z=57$), cerium (Ce, $Z=58$), praeodymium (Pr, $Z=59$), neodymium (Nd, $Z=60$) and samarium (Sm, $Z=62$) (see De Smedt et al. 2012; van Aarle et al. 2013; De Smedt et al. 2015, and references therein). Figure 6 shows the spectral regions that cover the strongest Ba II line at 6141.72 Å and a weaker line at 6496.90 Å. It can be clearly seen that these Ba lines are absent in the spectra therefore implying that J005252 is not *s*-process enriched. We used the strongest Ba II line at 6141.72 Å to determine an upper limit for Ba. We obtained a $[Ba/Fe] < 0.55$, for an assumed EW of 5 mÅ, which is above solar. We note that there is a mild *s*-process enrichment in the initial composition of the LMC, starting from solar value at $[Fe/H] = -1.5$ and reaching 0.8 for $[Fe/H] \geq -0.3$ (Van der Swaelmen et al. 2013). With the assumption that the SMC may also be mildly *s*-process enriched, it is very likely that J005252 is not *s*-process enriched.

Another chemical trend displayed by post-AGB stars is ‘depletion’. Affected photospheres are characterised by a selective depletion of refractory elements, while the

volatile elements retain their original abundance (see Section 1). The best elements to trace depletion are Zn and S (Van Winckel 2003). In Figure 7, we show the spectral regions that cover the Zn I line at 4810.50 Å and the S I lines at 6757.16 Å and 6748.79 Å. It can be seen that these lines cannot be detected in the spectra of J005252. At the T_{eff} of J005252 we do not expect to see Zn I. Therefore the absence of the strongest Zn I line at 4810.50 Å does not yield a useful upper limit for Zn. We used the strongest useful S I lines at 6757.16 Å and 6748.79 Å to quantify an upper limit for the S abundance. We estimated an upper limit of $[\text{S}/\text{Fe}] \leq 1.0$. The estimated upper limit for the S abundance and the lack of detectable S I lines (as shown in Figure 7) implies that J005252 does not show signs of depletion.

4. Understanding the photospheric chemistry of J005252

Detailed chemical abundance studies of post-AGB stars have shown that they are chemically much more diverse than anticipated and most of these chemical diversities have been tied to the evolutionary channels of these stars. For instance, some of the single post-AGB objects are the most C-rich and *s*-process enriched objects known to date while others, the likely binary objects, are not enriched at all and exhibit a photospheric depletion (see Section 1). The object of this study, J005252, has a rather intriguing chemistry which does not comply with any of the known chemical trends observed in post-AGB stars (see Van Winckel 2003, for a review), therefore making this object a chemically very peculiar star. In the following subsections we interpret the observed photospheric composition of J005252.

4.1. The carbon abundance of J005252

Based on the mid-IR excess (due to a detached circumstellar shell surrounding the central star, see Figure 1), low surface gravity ($\log g = 1.0 \pm 0.25$) and high luminosity ($L_{\text{ph}}/L_{\odot} = 8200 \pm 700$) and low metallicity ($[\text{Fe}/\text{H}] = -1.18 \pm 0.10$) of J005252, this object is very likely to be a post-AGB star. The high luminosity of the object points to the star having evolved off the TP-AGB phase (see Section 1). For this reason we expect the stellar photosphere to be enriched in carbon and probably enriched with *s*-process elements. However, this is not the case. J005252 is not C-enhanced (see Section 3.4 and Figure 5). There is no detectable carbon-enhancement. The oxygen is above solar with $[\text{O}/\text{Fe}] = 0.29 \pm 0.1$, after taking into account NLTE corrections. The lack of C-enhancement in this object indicates that the star did not undergo TDU episodes or the TDU was inefficient. We could not investigate the nitrogen abundance as the nitrogen lines lie outside the wavelength range of our spectra.

In the SMC, the observed carbon star luminosity function (CSLF), based on the detected AGB carbon stars, peaks at an $M_{\text{bol}} \approx -4.4$, (derived using the data presented in Groenewegen 2004). J005252 (with a luminosity of $8200 L_{\odot}$ corresponds to $M_{\text{bol}} = -5.03$) falls within one sigma of the peak of the CSLF suggesting that it should be enhanced in carbon.

TP-AGB evolutionary models allow for a wide exploration of the TDU characteristics as a function of stellar mass, metallicity and mass-loss descriptions (Karakas et al. 2002; Herwig 2000, 2004a,b; Weiss & Ferguson 2009; Karakas 2010; Cristallo et al. 2011; Fishlock et al. 2014). The predicted surface abundances are, however, subject to many uncertainties as they are not only dependent on the TDU physics itself, but also on the dilution of the remaining envelope material and hence on the adopted mass loss description. The latter will also determine the number of thermal pulses predicted for every model. In stars less than

$\sim 2.5 M_{\odot}$, the efficiency of TDU (commonly represented by λ which is the ratio between the mass dredged-up into the envelope and the core-mass growth during the interpulse period) has been predicted to increase with stellar mass as well as during the evolution on the AGB (Karakas 2010; Cristallo et al. 2011; Ventura et al. 2014; Marigo et al. 2013; Fishlock et al. 2014). Lower metallicities favour an earlier onset of TDU and a larger efficiency resulting in the formation of low-mass C-stars. Stellar evolution models (Karakas 2010; Fishlock et al. 2014) show that for an object such as J005252, (with an initial mass of $\sim 1.5 - 2 M_{\odot}$, and $Z=0.001$), the efficiency of TDU ranges between 0.4 to 0.7 with 10 to 14 TDU episodes with 14 to 17 computed thermal pulses. The COLIBRI model by Marigo et al. (2013), (with an initial mass of $\sim 1.5 - 2 M_{\odot}$, and $Z=0.001$), shows that the efficiency of TDU reaches a maximum of ~ 0.6 with 9 thermal pulses yielding a C/O of ~ 10 . For an initial mass of $\sim 1.5 - 2 M_{\odot}$, and $Z=0.001$, the models by (Ventura et al. 2014) predict that the efficiency of TDU reaches a maximum of ~ 0.9 with ~ 11 – thermal pulses, yielding a C/O of $\sim 7 - 13$. Therefore, the standard models predict that J005252 should be C-rich. This implies that J005252 should be enhanced in carbon.

Several synthetic models of the TP-AGB phase (e.g., Marigo et al. 1999; Stancliffe et al. 2005; Izzard et al. 2004) have been calculated to fit the observed carbon star luminosity function in the SMC. The synthetic models by Stancliffe et al. (2005), for the SMC metallicity ($Z=0.004$), find that carbon stars were formed in all their models with initial masses between $1 M_{\odot}$ and $3 M_{\odot}$. Their lowest mass models become carbon stars with $M_{\text{bol}} = -4.2$, which is only just below the peak of the SMC CSLF.

A process that does destroy the production of carbon in AGB stars is HBB (see Section 1). However, at $Z=0.001$ this is only active in stars with masses greater than $\sim 2.5 - 3 M_{\odot}$ (Boothroyd et al. 1993; Lattanzio 1992; Lattanzio et al. 1996; Karakas 2010; Ventura et al. 2012; Fishlock et al. 2014) and therefore is not likely to affect the

nucleosynthesis of J005252.

Therefore based on predictions from both detailed single stellar evolutionary models as well as synthetic TP-AGB evolution calculations, and based on the stellar parameters ($L_{\text{ph}}/L_{\odot} = 8200$, $[\text{Fe}/\text{H}] = -1.18 \pm 0.10$, $M/M_{\odot} = 1.5 - 2 M_{\odot}$, see Section 3), J005252 should be C-rich, but the observations do not agree with the predictions of any model found in the literature.

4.2. The *s*-process abundance of J005252

The SED of J005252 is of shell-type suggesting that this object is a single star. As mentioned in Section 1, the MC and Galactic post-AGB stars with shell-type SEDs often show C-enhancement and *s*-process enrichment. In Figure 8 we compare the spectral region covering the Ba II line at 6141.72 Å with the *s*-process enriched LMC post-AGB star J050632 (van Aarle et al. 2013) and the *s*-process enriched Galactic post-AGB star HD187885 (Van Winckel et al. 1996b). We chose these objects for our spectral comparison as they have stellar parameters (T_{eff} , $\log g$, $[\text{Fe}/\text{H}]$, see Table 5) similar to J005252. The LMC star (J050632) has a lower luminosity than J005252 while for the Galactic post-AGB star (HD187885) there is no luminosity estimate available. Our comparison (see Figure 8) shows that, despite the very similar stellar parameters between the three stars, J005252 is clearly not *s*-process enriched.

4.3. Is J005252 depleted?

Since J005252 does not follow the single star chemical evolutionary trends we consider the possibility of photospheric depletion. We perform a comparison of J005252 with a Galactic binary post-AGB star BD+394926 (Rao et al. 2012; Gezer et al. 2015). This is the

only known depleted Galactic post-AGB star with similar stellar parameters (see Table 5) to our object. BD+394926 is very affected by the depletion process which results in a $[\text{Fe}/\text{H}] = -2.4$. Post-AGB binaries have a $[\text{C}/\text{Fe}] > 0$ because the difference in condensation temperature between C and Fe during the depletion process leads to high $[\text{C}/\text{Fe}]$. However, J005252 does not show any traces of carbon in its photospheric composition. In Figure 9 we compare the spectral region covering the CI lines at 5380.34 Å and 6587.62 Å of our object to that of BD+39 4926. The spectra of BD+394926 shows the presence of the CI line while our object does not. In Figure 10 we show a comparison of the abundance analysis results ($[\text{X}/\text{Fe}]$ vs Z) of J005252 and BD+394926. As expected, BD+394926 has a high $[\text{C}/\text{Fe}]$ ratio. Furthermore, BD+394926 shows the presence of volatile elements like Zn and S, and a depletion of refractory elements that scale with Fe. J005252 shows no signs of a depleted photospheric composition (see Figure 10) and hence is unlikely to be in a binary system.

We conclude that J005252 is the first known object with a photospheric chemistry that does not comply with the standard theories of stellar evolution and nucleosynthesis. The well constrained luminosity and stellar parameters of this object, argue for its post-AGB evolutionary nature. It is the most luminous post-AGB star to be studied in detail to date.

Ironically, we note that J005252 may be the first star to be consistent with standard AGB evolutionary models. Initially, AGB models for low masses did not show the production of *s*-process elements because there was no ^{13}C -pocket formed without adding some form of partial mixing to the models. With observations making it clear that such mixing was occurring, various mechanisms were included in the models to produce such a pocket, and the subsequent enhancements in *s*-process elements. Likewise, the third dredge-up is notoriously difficult to predict quantitatively (Frost & Lattanzio 1996) In many cases some extra-mixing, or overshoot, was added to try to initiate dredge-up at low

masses, to make models consistent with the observations. It is perhaps amusing that we are now searching for an explanation as to why J005252 matches the original models, and not those that are constructed to fit the majority of stars.

5. Galactic Analogues of J005252

Since the Galactic sample is observationally well studied, we looked for analogues of J005252 amongst the known Galactic post-AGB stars. We were able to identify thick-disk objects: HD133656 and SAO239853. These two objects have very similar SED characteristics to J005252 (see Figure 11) and also similar stellar parameters (see Table 6). Figure 12 shows the similarity between the spectra of the three stars. The photospheric chemistry of HD133656 and SAO239853 were studied in detail by Van Winckel et al. (1996a) and Van Winckel (1997), respectively. In Figure 13 we plot the $[X/Fe]$ vs atomic mass (Z) for the three objects. We find that all three objects show similar trends in their photospheric chemistry (see Figure 13), with J005252 being the most extreme case in terms of an unusual chemistry. In this section we summarise the abundance results of the two objects.

HD133656 was first identified as a high-latitude metal-deficient star by Van Winckel et al. (1996a). The photometry, IUE spectrum, $H\gamma$ and $H\beta$ line profiles all agree very well with an effective temperature of about 8000 K and a $\log g$ of 1.0. The study by Van Winckel et al. (1996a) showed that this star is metal poor ($[Fe/H] \approx -1.00$) but with $[C/Fe] = +0.3$, $[N/Fe] = +0.7$ and $[O/Fe] = +0.5$. The oxygen abundance follows the oxygen content of unevolved Galactic stars of the same metallicity. The light α -elements (Mg, Si, S) yield a $[\alpha/Fe] = +0.45$. The heavier α -element Ca follows the Fe deficiency, and so do the Fe-peak elements Sc, Ti, Cr and Ni. No s -process overabundances were detected.

SAO239853 was first classified as a post-AGB candidate star by Hrivnak et al. (1989) on the basis of the IRAS colours. It is a pulsating variable with a period of 37 days and a total amplitude of 0.103 magnitudes in V -band (Bogaert 1994). The study by Van Winckel (1997) showed that this object is metal-deficient with an Fe abundance between -0.8 and -1.0 . The atmosphere is C and N rich, with a $[\text{C}/\text{Fe}] = +0.4$, and $[\text{N}/\text{Fe}] = +0.5$. The O abundance of $[\text{O}/\text{Fe}] = +0.6$ to $+0.7$ is about 0.2 dex higher than expected for an unevolved object with $[\text{Fe}/\text{H}]$ between -0.8 to -1.0 , indicating a slight O enrichment. The star was identified to have a s -process element deficiency based on two small lines of Zr and two lines of Ba, which yields a $[\text{s}/\text{Fe}]$ between -0.3 and -0.4 .

Amongst the observed sample of post-AGB stars whose chemistry has been studied in detail these two objects are the best known Galactic analogues of J005252. The C-enhancement in these stars is in the order of $+0.3$ for HD133656 and $+0.4$ for SAO239853. For metallicities of around $[\text{Fe}/\text{H}] = -1.0$, stars with thick-disc kinematics have $[\text{C}/\text{Fe}] \approx 0.2$ (Nissen et al. 2014). This suggests that these two stars exhibit a photospheric composition with no strong C-enhancement. These stars also do not show a strong s -process enrichment or a photospheric depletion. In these stars, the lack of a nucleosynthetic history that reflects the third dredge-up was previously associated with the possibility that their initial mass was too low for active nucleosynthesis enrichment on the AGB (Van Winckel et al. 1996b). Another possibility is that the objects are indeed of low luminosity and are associated with the recently identified post-RGB stars (see Kamath et al. 2016, and Section 1).

As mentioned in Section 1, the recent first Gaia data release, (Gaia DR1, Gaia Collaboration et al. 2016), has provided parallaxes for some Galactic post-AGB stars. Parallaxes are available for both HD133656 and SAO239853. For SAO239853, the error in parallax (0.34 mas) is twice the parallax (0.15 mas), which results in a large variation in luminosity (ranging from $1200 L_{\odot}$ to $14000 L_{\odot}$). Therefore, we are unable to comment

whether SAO239853 is a post-AGB or post-RGB object. In the case of HD133656, the error in parallax (0.34 mas) is around one third of the parallax (1.10 mas). However, this translates into a luminosity that ranges between 800 L_{\odot} and 2800 L_{\odot} , which implies that the evolutionary nature of HD133656 remains uncertain. With future data releases from Gaia, which promise more accurate parallaxes, we should soon be able to obtain accurate distances and hence luminosities of these likely Galactic analogues to confirm their evolutionary nature and therefore their chemical peculiarities.

6. Conclusions

Atmospheres of post-AGB stars contain all the chemical enrichment from internal nucleosynthesis that has occurred during the entire AGB phase and therefore serve as excellent probes to understand stellar evolution and nucleosynthesis. Galactic post-AGB stars have been found to be chemically much more diverse than anticipated. Some objects are the most *s*-process enriched objects known to date while others are not enriched at all. However, the poorly known distances (and hence luminosities and masses) of the Galactic post-AGB sample hamper the interpretation of their abundances in the broader theoretical context of stellar evolution. Due to their known distances, MC post-AGB stars provide excellent constraints and offer unprecedented tests for AGB theoretical evolution and nucleosynthesis models of low- and intermediate-mass stars. Our recent search for MC post-AGB stars (Kamath et al. 2014, 2015, in the SMC and LMC, respectively) yielded a spectroscopically verified catalogue of optically visible post-AGB stars. We are currently doing follow-up high-resolution detailed chemical abundance studies of a few of these objects, one of which is J005252.

In this paper, we argue for the likely post-AGB nature of J005252 and present a detailed photospheric study of this object which revealed its intriguing photospheric composition.

This luminous ($8200 \pm 700 L_{\odot}$), metal-poor ($[\text{Fe}/\text{H}] = -1.18 \pm 0.10$) star with a shell-type SED, provides the first observational evidence for a star that fails the third dredge-up. This object with $T_{\text{eff}} = 8250 \pm 250 \text{ K}$, $\log g = 1.0 \pm 0.25 \text{ dex}$, and $\xi_t = 2.0 \pm 0.25 \text{ kms}^{-1}$, shows no traces of carbon-enhancement, indicating that this low-metallicity, low initial mass (1.5 to $2.0 M_{\odot}$) object has not undergone any third dredge-up episode during its entire AGB phase. The oxygen is above solar with $[\text{O}/\text{Fe}] = 0.29 \pm 0.1$, after taking into account NLTE corrections. Furthermore, J005252 shows neither signs of an *s*-process enrichment, which is characteristic of single post-AGB stars, nor a depleted photospheric chemistry which is characteristic of most binary post-AGB stars.

Assuming that J005252 is a single star, stellar evolution and nucleosynthesis models (Lattanzio 1986, 1989; Karakas 2010; Cristallo et al. 2011; Fishlock et al. 2014) that are appropriate for J005252 (based on its luminosity, initial mass and metallicity) predict this object to undergo third dredge-up and become C-rich. Synthetic models of TP-AGB stars that are calculated to fit the SMC CSLF also predict a star with the luminosity and metallicity of J005252 to be C-rich.

We consider the possibilities of nucleosynthetic process, such as HBB (Boothroyd et al. 1993; Lattanzio 1992; Lattanzio et al. 1996) that can prevent the formation of high-luminosity carbon stars. However, at the metallicity of J005252 ($Z = 0.001$), HBB is only active in stars with $M \gtrsim 2.5 M_{\odot}$ (Ventura et al. 2014). Since J005252 is star with $M \approx 1.5 - 2 M_{\odot}$ and $Z = 0.001$, it is likely that the temperature at the base of the convective envelope during the interpulse period is not high enough to activate HBB.

Therefore, the only way to explain the intriguing chemistry of J005252 is via some mechanism that results in an AGB life without dredge-up episodes. Alternatively, this object could be a product of a merger scenario wherein it is not easy to trace the merger process and therefore understand the nucleosynthetic history of the end-product. However,

the spectral lines of J005252 are resolved and do not show signs of strong rotation, which is normally a characteristic feature of mergers.

In our attempt to find Galactic analogues, we found two stars: SAO239853 and HD133656, which are likely to also have failed the third dredge-up. However, their uncertain luminosities bring in the possibility of them being post-RGB stars and therefore restricts us from confirming the possibility of a failed TDU in these stars.

J005252 is the first detected object of its kind. This object along with its two likely Galactic analogues opens up a possibility for a new evolutionary channel or unknown mass-loss and/or nucleosynthetic processes that govern the AGB phase. One of the useful probes of better understanding the chemistry of J005252 is the N abundance as it is affected via the CNO cycle. Our current spectral region does not cover usable N lines. We aim to obtain spectra covering the N lines to be able to determine if whether the N abundance can give us hints for solving the nucleosynthetic mystery of J005252.

7. Acknowledgments

DK and HVW acknowledge the support of the KU Leuven contract GOA/13/012. DK acknowledges the support of the FWO grant G.OB86.13. PRW has received support from the Australian Research Council Discovery Project DP120103337.

Facilities: This study is based on observations collected with the Very Large Telescope at the ESO Paranal Observatory (Chile) of programme number 092.D-0485

REFERENCES

- Amarsi, A. M., Lind, K., Asplund, M., Barklem, P. S., & Collet, R. 2016, MNRAS, 463, 1518
- Asplund, M. 2005, ARA&A, 43, 481
- Asplund, M., Grevesse, N., Sauval, A. J., & Scott, P. 2009, ARA&A, 47, 481
- Bertelli, G., Girardi, L., Marigo, P., & Nasi, E. 2008, A&A, 484, 815
- Bogaert, E. 1994, PhD thesis, PhD thesis. Kathol. Univ. Leuven , (1994)
- Bolatto, A. D., Simon, J. D., Stanimirović, S., et al. 2007, ApJ, 655, 212
- Boothroyd, A. I., Sackmann, I.-J., & Ahern, S. C. 1993, ApJ, 416, 762
- Bujarrabal, V., Alcolea, J., Van Winckel, H., Santander-García, M., & Castro-Carrizo, A. 2013a, A&A, 557, A104
- Bujarrabal, V., Castro-Carrizo, A., Alcolea, J., & Van Winckel, H. 2015, A&A, 575, arXiv:1502.01607
- Bujarrabal, V., Castro-Carrizo, A., Alcolea, J., et al. 2013b, A&A, 557, L11
- Busso, M., Gallino, R., Lambert, D. L., Travaglio, C., & Smith, V. V. 2001, ApJ, 557, 802
- Cardelli, J. A., Clayton, G. C., & Mathis, J. S. 1989, ApJ, 345, 245
- Castelli, F., & Kurucz, R. L. 2003, in IAU Symposium, Vol. 210, Modelling of Stellar Atmospheres, ed. N. Piskunov, W. W. Weiss, & D. F. Gray, 20P
- Cristallo, S., Straniero, O., Piersanti, L., & Gobrecht, D. 2015, ApJS, 219, 40
- Cristallo, S., Piersanti, L., Straniero, O., et al. 2011, ApJS, 197, 17

- De Propriis, R., Rich, R. M., Mallery, R. C., & Howard, C. D. 2010, *ApJ*, 714, L249
- de Ruyter, S., Van Winckel, H., Maas, T., et al. 2006, *A&A*, 448, 641
- De Smedt, K., Van Winckel, H., Kamath, D., & Wood, P. R. 2015, *A&A*, 583, A56
- De Smedt, K., Van Winckel, H., Karakas, A. I., et al. 2012, *A&A*, 541, A67
- Dekker, H., D’Odorico, S., Kaufer, A., Delabre, B., & Kotzlowski, H. 2000, in *Society of Photo-Optical Instrumentation Engineers (SPIE) Conference Series*, Vol. 4008, Society of Photo-Optical Instrumentation Engineers (SPIE) Conference Series, 534–545
- Deroo, P., Reyniers, M., Van Winckel, H., Goriely, S., & Siess, L. 2005, *A&A*, 438, 987
- Deroo, P., Van Winckel, H., Verhoelst, T., et al. 2007, *A&A*, 467, 1093
- Fishlock, C. K., Karakas, A. I., Lugaro, M., & Yong, D. 2014, *ApJ*, 797, 44
- Frost, C. A., & Lattanzio, J. C. 1996, *ApJ*, 473, 383
- Gaia Collaboration, Brown, A. G. A., Vallenari, A., et al. 2016, *ArXiv e-prints*, arXiv:1609.04172
- Geballe, T. R., Noll, K. S., Whittet, D. C. B., & Waters, L. B. F. M. 1989, *ApJ*, 340, L29
- Gezer, I., Van Winckel, H., Bozkurt, Z., et al. 2015, *MNRAS*, 453, 133
- Gielen, C., Van Winckel, H., Min, M., Waters, L. B. F. M., & Lloyd Evans, T. 2008, *A&A*, 490, 725
- Gielen, C., Van Winckel, H., Reyniers, M., et al. 2009, *A&A*, 508, 1391
- Gielen, C., Bouwman, J., van Winckel, H., et al. 2011, *A&A*, 533, A99

- Giridhar, S., Lambert, D. L., & Gonzalez, G. 2000, *ApJ*, 531, 521
- Groenewegen, M. A. T. 2004, *A&A*, 425, 595
- Guzmán-Ramírez, L., Zijlstra, A. A., Níchuimín, R., et al. 2011, *MNRAS*, 414, 1667
- Herwig, F. 2000, *A&A*, 360, 952
- . 2004a, *ApJ*, 605, 425
- . 2004b, *ApJS*, 155, 651
- . 2005, *ARA&A*, 43, 435
- Hillen, M., Verhoelst, T., Van Winckel, H., et al. 2013, *A&A*, 559, A111
- Hrivnak, B. J., Kwok, S., & Volk, K. M. 1989, *ApJ*, 346, 265
- Izzard, R. G., Tout, C. A., Karakas, A. I., & Pols, O. R. 2004, *MNRAS*, 350, 407
- Kamath, D., Wood, P. R., & Van Winckel, H. 2014, *MNRAS*, 439, 2211
- . 2015, *ArXiv e-prints*, arXiv:1508.00670
- Kamath, D., Wood, P. R., Van Winckel, H., & Nie, J. D. 2016, *A&A*, 586, L5
- Karakas, A. I. 2010, *MNRAS*, 403, 1413
- Karakas, A. I., & Lattanzio, J. C. 2007, *PASA*, 24, 103
- . 2014, *PASA*, 31, e030
- Karakas, A. I., Lattanzio, J. C., & Pols, O. R. 2002, *PASA*, 19, 515
- Keller, S. C., & Wood, P. R. 2006, *ApJ*, 642, 834
- Klochova, V. G. 1995, *MNRAS*, 272, 710

- Kupka, F., Piskunov, N., Ryabchikova, T. A., Stempels, H. C., & Weiss, W. W. 1999, A&AS, 138, 119
- Kwok, S., Volk, K. M., & Hrivnak, B. J. 1989, ApJ, 345, L51
- Lattanzio, J., Frost, C., Cannon, R., & Wood, P. R. 1996, Mem. Soc. Astron. Italiana, 67, 729
- Lattanzio, J. C. 1986, ApJ, 311, 708
- . 1989, ApJ, 344, L25
- . 1992, PASA, 10, 120
- Lewis, I. J., Cannon, R. D., Taylor, K., et al. 2002, MNRAS, 333, 279
- Luck, R. E., Bond, H. E., & Lambert, D. L. 1990, ApJ, 357, 188
- Luck, R. E., Moffett, T. J., Barnes, III, T. G., & Gieren, W. P. 1998, AJ, 115, 605
- Maas, T., Van Winckel, H., & Lloyd Evans, T. 2005, A&A, 429, 297
- Marigo, P., Bressan, A., Nanni, A., Girardi, L., & Pumo, M. L. 2013, MNRAS, 434, 488
- Marigo, P., Girardi, L., & Bressan, A. 1999, A&A, 344, 123
- Meixner, M., Gordon, K. D., Indebetouw, R., et al. 2006, AJ, 132, 2268
- Min, M., Jeffers, S. V., Canovas, H., et al. 2013, A&A, 554, A15
- Neilson, H. R., Ngeow, C.-C., Kanbur, S. M., & Lester, J. B. 2009, ApJ, 692, 81
- Nie, J. D., Wood, P. R., & Nicholls, C. P. 2012, MNRAS, 423, 2764
- Nissen, P. E., Chen, Y. Q., Carigi, L., Schuster, W. J., & Zhao, G. 2014, A&A, 568, A25

- Rao, S. S., Giridhar, S., & Lambert, D. L. 2012, MNRAS, 419, 1254
- Reddy, B. E., Lambert, D. L., Gonzalez, G., & Yong, D. 2002, ApJ, 564, 482
- Reyniers, M., van de Steene, G. C., van Hoof, P. A. M., & Van Winckel, H. 2007, A&A, 471, 247
- Reyniers, M., & Van Winckel, H. 2003, A&A, 408, L33
- Romaniello, M., Primas, F., Mottini, M., et al. 2005, A&A, 429, L37
- Snedden, C. A. 1973, PhD thesis, University of Texas at Austin
- Stancliffe, R. J., Izzard, R. G., & Tout, C. A. 2005, MNRAS, 356, L1
- Tognelli, E., Prada Moroni, P. G., & Degl’Innocenti, S. 2011, A&A, 533, A109
- van Aarle, E., Van Winckel, H., De Smedt, K., Kamath, D., & Wood, P. R. 2013, A&A, 554, A106
- van Aarle, E., Van Winckel, H., Lloyd Evans, T., et al. 2011, A&A, 530, A90+
- Van der Swaelmen, M., Hill, V., Primas, F., & Cole, A. A. 2013, A&A, 560, A44
- Van Winckel, H. 1997, A&A, 319, 561
- . 2003, ARA&A, 41, 391
- Van Winckel, H., Oudmaijer, R. D., & Trams, N. R. 1996a, A&A, 312, 553
- Van Winckel, H., & Reyniers, M. 2000, A&A, 354
- Van Winckel, H., Waelkens, C., & Waters, L. B. F. M. 1996b, A&A, 306, L37
- Van Winckel, H., Waelkens, C., Waters, L. B. F. M., et al. 1998, A&A, 336

- Vassiliadis, E., & Wood, P. R. 1994, *ApJS*, 92, 125
- Ventura, P., Dell’Agli, F., Schneider, R., et al. 2014, *MNRAS*, 439, 977
- Ventura, P., Karakas, A. I., Dell’Agli, F., et al. 2015, *MNRAS*, 450, 3181
- Ventura, P., Criscienzo, M. D., Schneider, R., et al. 2012, *MNRAS*, 424, 2345
- Volk, K., Kwok, S., & Hrivnak, B. J. 1999, *ApJ*, 516, L99
- Waters, L. B. F. M., Trams, N. R., & Waelkens, C. 1992, *A&A*, 262
- Weiss, A., & Ferguson, J. W. 2009, *A&A*, 508, 1343
- Witt, A. N., Vijh, U. P., Hobbs, L. M., et al. 2009, *ApJ*, 693, 1946
- Wood, P. R., & Zarro, D. M. 1981, *ApJ*, 247, 247

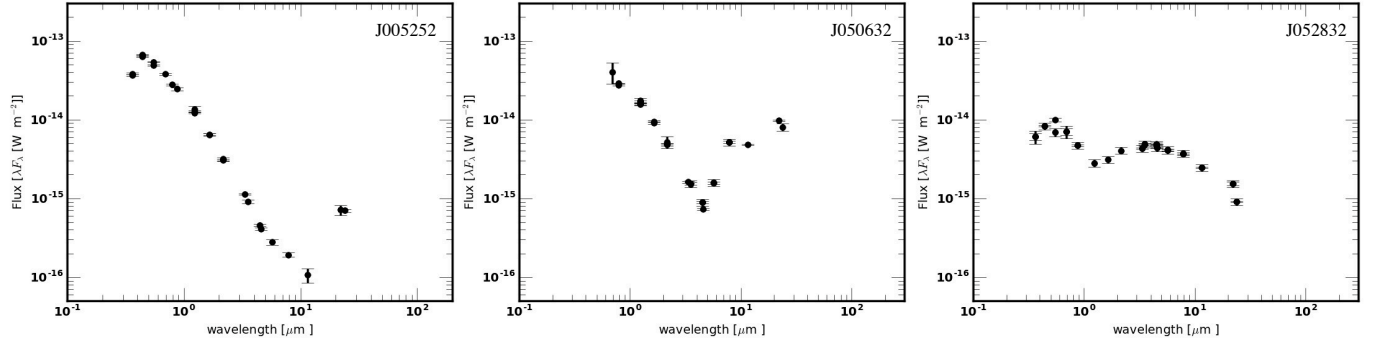


Fig. 1.— Left panel: SED of J005252. Center panel: SED of J050632.10-714229.8, a LMC shell-type source (van Aarle et al. 2013). Right panel: SED of J052832.60-690440.6, a LMC disc-type source (Kamath et al. 2015). The black symbols indicate the broadband photometry corrected for foreground extinction.

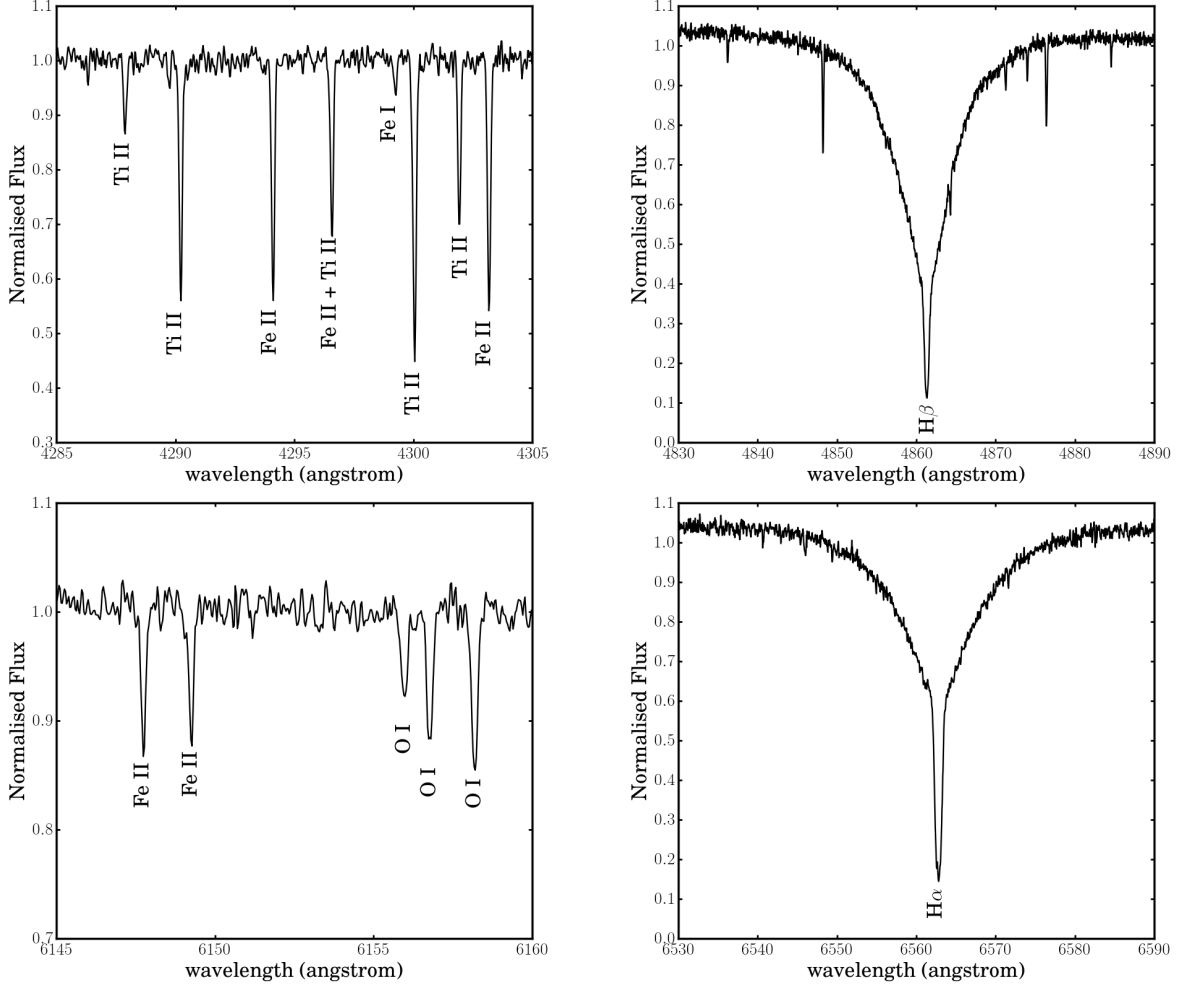


Fig. 2.— Spectral samples of J005252. The top-left panel shows a spectral region in the blue part of the spectra with lines of titanium (Ti) and iron (Fe). The top-right panel shows the $H\beta$ line at 4861.36 Å. The bottom-left panel shows the spectral region that contains neutral oxygen lines, the O I triplet, at 6155.97, 6156.78 and 6158.19 Å. The bottom-right panel shows the $H\alpha$ line at 6562.80 Å.

Table 1: Target details and overview of observations.

Star	RA	DEC	Exp.time (s)	Exp time (s)	V	L_{obs}/L_{\odot}	RV
	(J2000)	(J2000)	Blue Arm	Red Arm	mag		kms^{-1}
J005252	00:52:52.87	-72:28:42.9	3×1500	3×1500	14.031	8000	149 ± 1

Note. — ‘Exp.Time’ represents the exposure time. The Red arm is the combination of the lower and upper part of the mosaic CCD chip. V represents the V -band magnitude, L_{obs}/L_{\odot} is the observed luminosity corrected for foreground extinction, RV represents the heliocentric radial velocity (see text for details).

Table 2: Spectroscopically determined atmospheric parameters of J005252.

Stellar Parameters	J05252 _{UVES}	J005252 _{AAO}
T_{eff} (K)	8250 ± 250	7600 ± 500
$\log g$ (dex)	1.0 ± 0.25	1.4 ± 0.50
ξ_t (kms ⁻¹)	2.0 ± 0.25	-
[Fe I/H]	-1.05 ± 0.34	-
[Fe I/H] _{NLTE}	-0.87 ± 0.34	-
[Fe II/H]	-1.18 ± 0.10	-
[Fe/H]	-1.18 ± 0.10	-2.00 ± 0.5
N_{FeI}	34	-
N_{FeII}	31	-
$E(B-V)$	0.02 ± 0.02	0.02 ± 0.02
L_{ph}/L_{\odot}	8200 ± 700	7500
M/M_{\odot}	0.63 ± 0.02	0.62

Note. — J05252_{UVES} represents the spectroscopically determined atmospheric parameters of J005252 obtained using the UVES spectra presented in this study. J005252_{AAO} represents the spectroscopically determined atmospheric parameters of J005252 obtained using the low-res optical AAOmega spectra presented in (Kamath et al. 2014). We take the estimated [Fe II/H] value as the metallicity ([Fe/H]) of the star. [Fe I/H]_{NLTE} represents the value of [Fe I/H] after taking into account the NLTE effects for Fe I. We note that the NLTE effects for Fe II are negligible (see Section 3.1 for full details). The errors for [Fe/H] include line to line scatter and model uncertainty. N_{FeI} and N_{FeII} show the number of lines used for Fe I and Fe II respectively. Note: Assumed solar [Fe/H] = 7.50 dex (Asplund et al. 2009). L_{ph}/L_{\odot} represents the photospheric luminosity of J005252 and M/M_{\odot} is the derived mass of J005252 (see Section 3.2 for details).

Table 3: The linelist of J005252.87-722842.9.

Ion	λ	EP	log gf	EW	Abundance
8.0	6155.971	10.740	-0.670	19.40	8.258
8.0	6156.778	10.740	-0.450	26.80	8.220
8.0	6158.187	10.740	-0.310	33.70	8.219
12.0	5167.320	2.700	-0.750	45.80	6.596
12.0	5528.420	4.350	-0.470	9.10	6.577

Ion denotes the atomic number of the respective element along with the ionisation stage. λ represents the rest frame wavelength (in \AA), EP is the excitation potential in eV, log gf is the oscillator strength, EW is the equivalent width in m \AA . The full table is available as online supporting information.

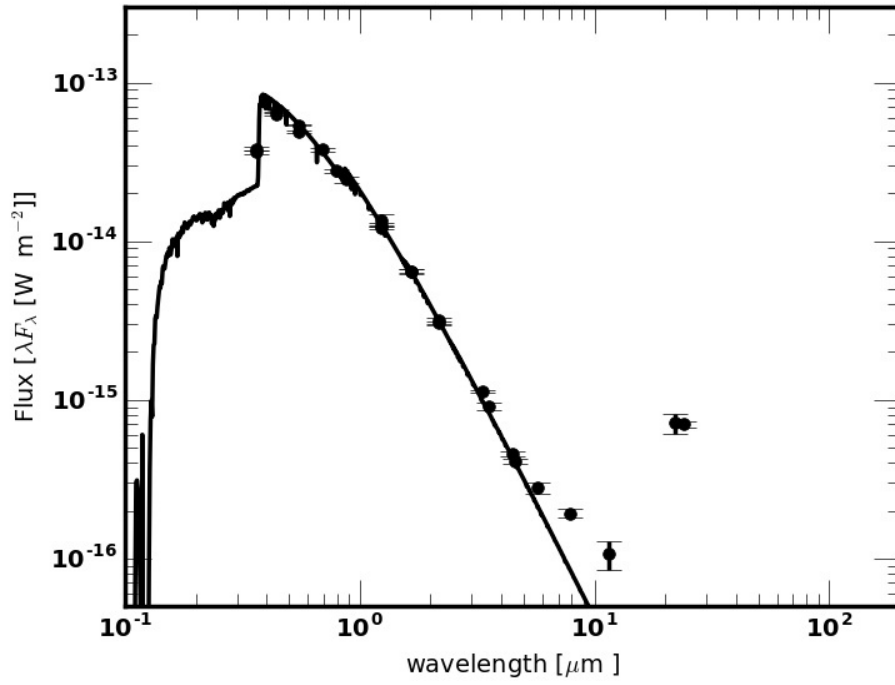


Fig. 3.— Spectral energy distribution for J005252. The black symbols represent the dereddened photometry. The black line represents the best-fitting scaled Kurucz model atmosphere (see text for details).

Table 4: Abundance results of J005252.

Ion	Z	N	$\log \epsilon_{\odot}$	$\log \epsilon$	σ_{121}	[X/H]	$\sigma_{\text{tot}}[\text{X}/\text{H}]$	[X/Fe]	$\sigma_{\text{tot}}[\text{X}/\text{Fe}]$
O I	8	3	8.69	8.23	0.06	−0.47	0.06	0.71	0.1
O I _{NLTE}	8	3	8.69	8.23	0.06	−0.89	0.06	0.29	0.1
Mg I	12	6	7.6	6.55	0.19	−1.05	0.30	0.13	0.17
Mg II	12	3	7.6	6.71	0.12	−0.89	0.10	0.29	0.14
Si II	14	5	7.51	6.60	0.34	−0.92	0.29	0.26	0.28
Sc II	21	1	3.15	2.18	0.2	−0.97	0.44	0.21	0.45
Ti II	22	23	4.95	3.92	0.4	−1.03	0.39	0.15	0.38
V II	23	5	3.93	2.83	0.1	−1.1	0.34	0.08	0.35
Cr I	24	3	5.64	4.73	0.19	−0.91	0.32	0.27	0.19
Cr II	24	15	5.64	4.63	0.09	−1.01	0.3	0.17	0.3
Fe I	26	34	7.5	6.39	0.11	−1.05	0.34	0.13	0.07
Fe I _{NLTE}	26	34	7.5	6.39	0.11	−0.87	0.31	0	0.07
Fe II	26	39	7.5	6.48	0.08	−1.18	0.10	0	0.05
Ni II	28	2	6.22	5.19	0.18	−1.03	0.32	0.15	0.31
C I	6		8.43	7.69		< −0.66		< 0.50	
Ba II	56		2.18	1.55		< −0.63		< 0.55	

The first column gives the ions that were detected and studied. The second column gives their corresponding atomic number. N is the number of lines used for each ion. $\log \epsilon_{\odot}$ are the solar abundances of the elements from Asplund et al. (2009), $\log \epsilon$ is the determined abundance, σ_{121} is the line-to-line scatter, [X/Fe] is the element-over-iron (Fe II) ratio, [X/H] is the element-over-hydrogen ratio, and $\sigma_{\text{tot}}[\text{X}/\text{H}]$ and $\sigma_{\text{tot}}[\text{X}/\text{Fe}]$ is the total uncertainty on [X/H] and [X/Fe], respectively. We impose a σ_{121} of 0.20 dex for all ions for which only one line is available for the abundance determination. [Fe I/H]_{NLTE} and O I_{NLTE} represents the values after taking into account the NLTE effects for Fe I. We note that the NLTE effects for Fe II are negligible and unknown for other elements (see Section 3.1 for full details). We note that the abundances of C (Z = 6) and Ba (Z = 56) are upper limits. See text for further details.

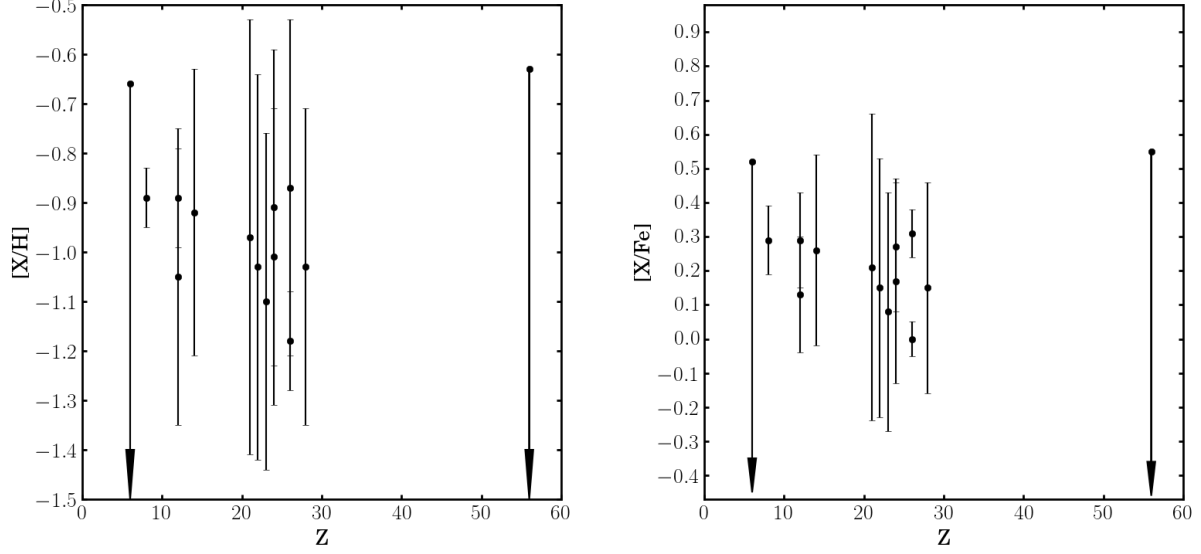


Fig. 4.— Left panel: element over hydrogen $[X/H]$ ratios of J005252. The error bars represent the total uncertainties σ_{tot} in $[X/H]$. Right panel: element over iron $[X/Fe]$ ratios of J005252. The errors bars represent the total uncertainties σ_{tot} in $[X/Fe]$. Note: the abundances of C ($Z=6$) and Ba ($Z=56$) are upper limits and marked with downward arrows.. For some of the elements we were able to estimate abundances using both neutral and singly-ionised lines. For such cases, we show both the abundances. For O I and Fe I we plot their abundances corrected for NLTE effects (see Table 4).

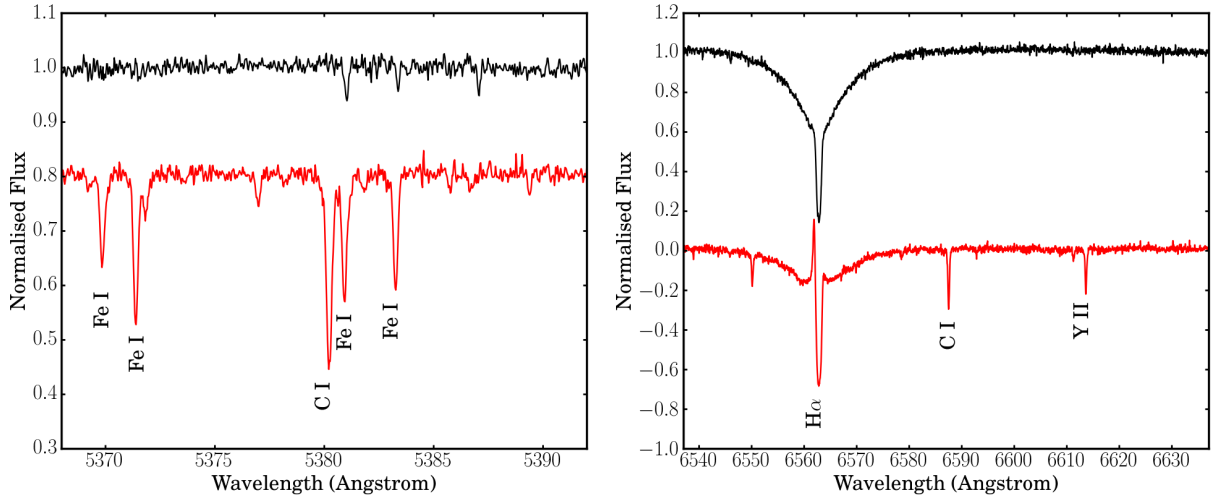


Fig. 5.— Normalised spectra of J005252 (in black) covering the region that contains strong neutral carbon (CI) lines at 5380.34 Å (left panel) and 6587.62 Å, (right panel). The spectra of J050632.10-714229.8 (in red), a known *s*-process enriched, single LMC post-AGB star, with similar stellar parameters to J005252, is shown for comparison. See text for further details.

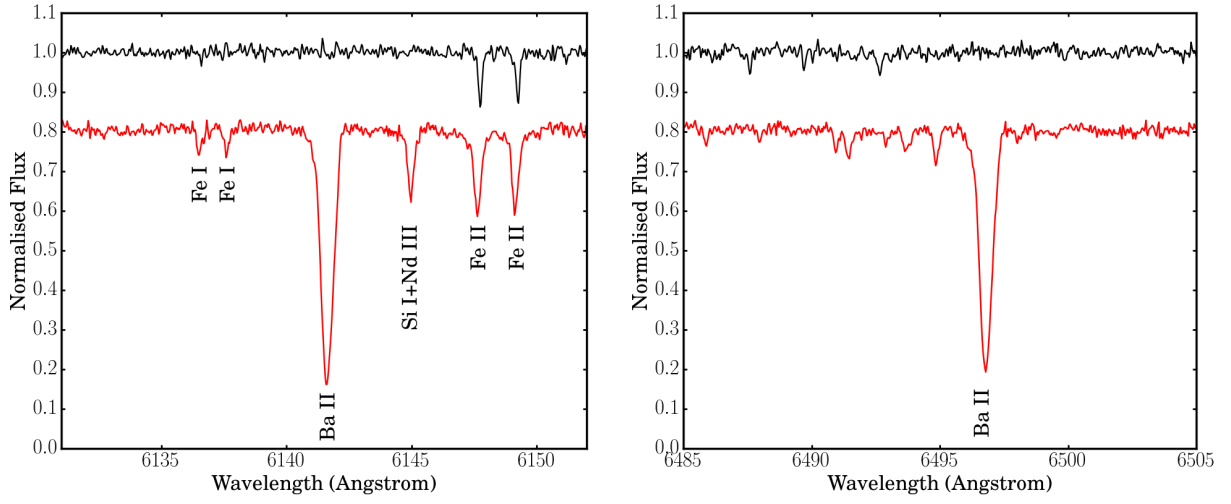


Fig. 6.— Normalised spectra of J005252 (in black) covering the region that contains strong singly ionised barium (Ba II) lines at 6141.72 Å (left panel) and 6496.90 Å (right panel). The spectra of J050632.10-714229.8 (in red), a known *s*-process enriched, single LMC post-AGB star, with similar stellar parameters to J005252, is shown for comparison. See text for further details.

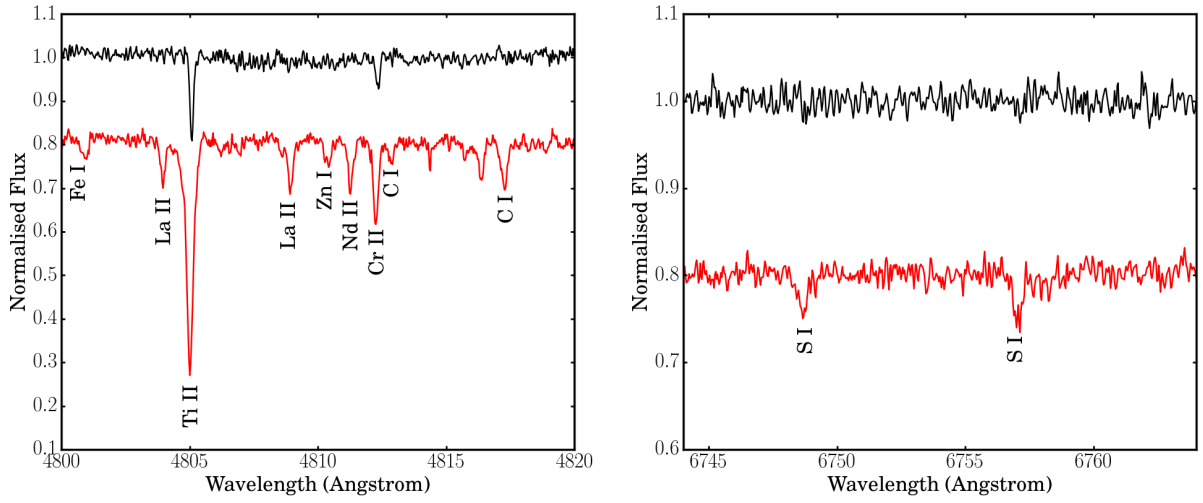


Fig. 7.— Normalised spectra of J005252 (in black) covering the region that contain a strong neutral zinc (Zn I) line at 4810.50 Å (left panel) and neutral sulphur (S I) lines at 6757.16 Å and 6748.79 Å (right panel). The spectra of J050632.10-714229.8 (in red), a known *s*-process enriched, single LMC post-AGB star, with similar stellar parameters to J005252, is shown for comparison. See text for further details.

Table 5: Atmospheric parameters of J005252, J050632, HD187885 and BD+394926.

Stellar Parameters	J052522	J050632	HD187885	BD+394926
Host galaxy	SMC	LMC	Milky Way	Milky Way
T_{eff} (K)	8250 ± 250	6750 ± 125	6750 ± 125	7750 ± 250
$\log g$ (dex)	1.00 ± 0.25	1.0 ± 0.25	1.5 ± 0.25	1.0 ± 0.5
ξ_t (kms $^{-1}$)	2.0 ± 0.25	3.0 ± 0.25	5.0 ± 0.25	3.0 ± 0.5
[Fe/H]	-1.18 ± 0.10	-1.22 ± 0.16	-0.5 ± 0.20	-2.37 ± 0.20
$E(B-V)$	0.02 ± 0.02	0.05 ± 0.06	-	-
L_{ph}/L_{\odot}	8200 ± 700 ,	5400 ± 700	-	-

Note. — Columns 1,2,3 and 4 list the spectroscopically determined atmospheric parameters of J005252, J050632, HD187885 and BD+394926 obtained using the UVES spectra presented in this study, from van Aarle et al. (2013), from Van Winckel et al. (1996b) and from Rao et al. (2012), respectively. We note that for the Galactic objects HD187885 and BD+394926 there are no luminosity and $E(B-V)$ measurements available.

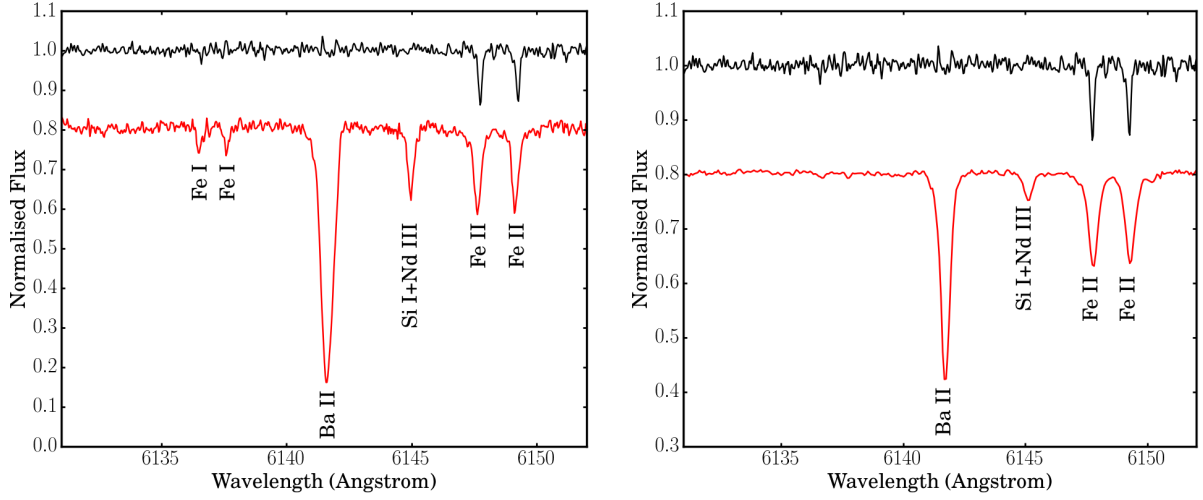


Fig. 8.— Normalised spectra of J005252 (in black) covering the region that contains the singly ionised barium (Ba II) line at 6141.72 Å. The left panel shows the spectra of J050632.10-714229.8 (in red), a known *s*-process enriched, single post-AGB star in the LMC with similar stellar parameters to J005252. The right panel shows the spectra of HD187885 (in red), a known Galactic *s*-process enriched, single post-AGB star with similar stellar parameters to J00525. See text for more details.

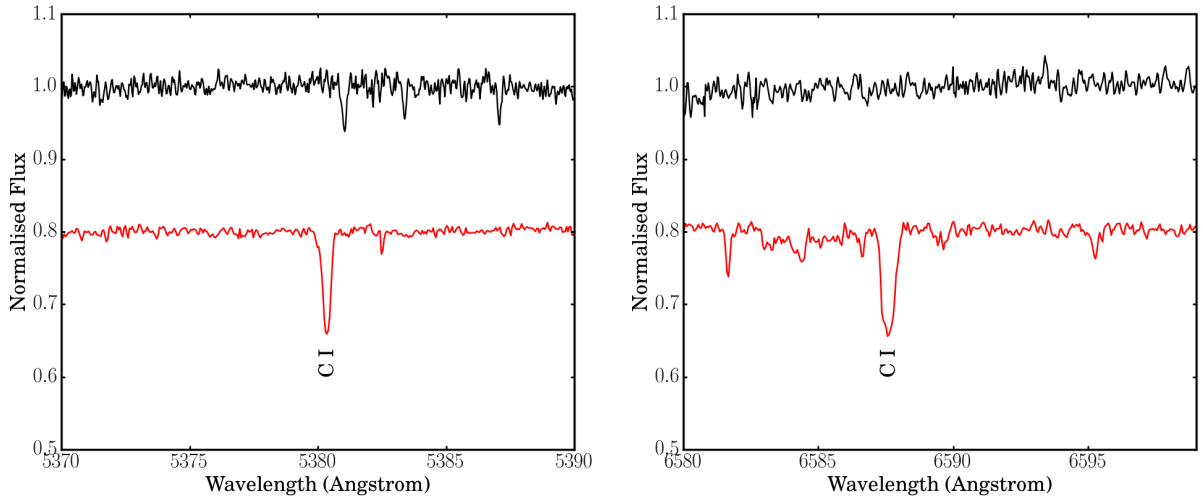


Fig. 9.— Normalised spectra of J005252 (in black) covering the region that contains the neutral carbon line (C I) line at 5380.34 Å (left panel) and 6587.62 (right panel). In both the plots we show the spectra of a known binary post-AGB star BD+394926 (in red), with a depleted photospheric chemistry, for comparison.

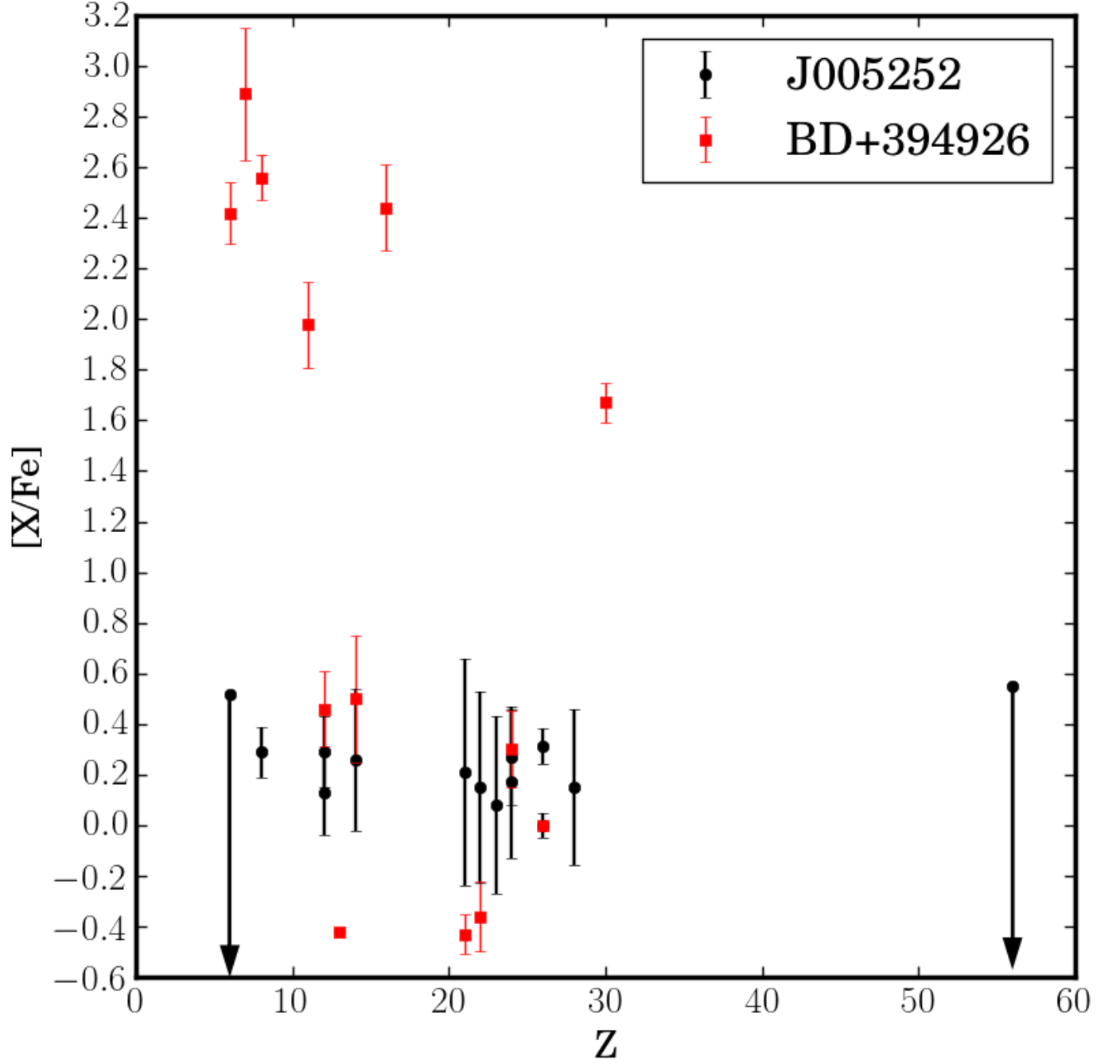


Fig. 10.— Element over iron $[X/Fe]$ ratios for J005252 (in black) and BD+394926 (in red). Note: For J005252, the abundances of C ($Z=6$) and Ba ($Z=56$) are upper limits and marked with downward arrows. For J005252, the O I and Fe I we plot are the abundances corrected for NLTE effects (see Table 4)

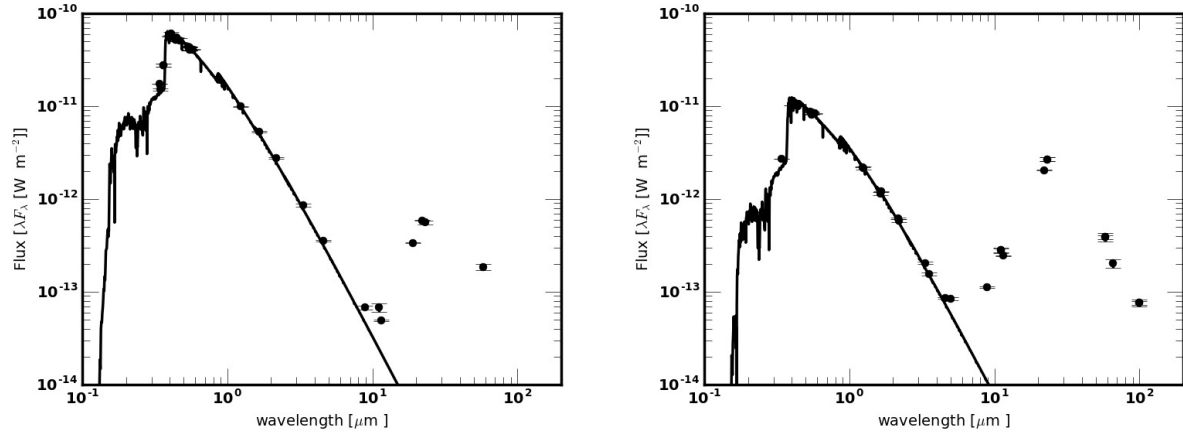


Fig. 11.— Spectral energy distribution of the two likely Galactic analogues of J005252: HD133656 (left panel) and SAO239854 (right panel). The black symbols indicate the broad-band photometry corrected for foreground extinction.

Table 6: Atmospheric parameters of J005252 and its likely Galactic analogues: HD133656 and SAO239853.

Stellar Parameters	J005252	HD133656	SAO239853
Host galaxy	SMC	Milky Way	Milky Way
T_{eff} (K)	8250 ± 250	8000 ± 125	7500 ± 125
$\log g$ (dex)	1.0 ± 0.25	1.0 ± 0.25	1.0 ± 0.25
ξ_{t} (kms $^{-1}$)	2.0 ± 0.25	6.0 ± 0.25	5.0 ± 0.25
[Fe/H]	-1.18 ± 0.10	-1.0 ± 0.16	-0.8 ± 0.20
$E(B-V)$	0.02 ± 0.02	-	-
L_{ph}/L_{\odot}	8200 ± 700	-	-

Note. — Columns 1,2 and 3 list the spectroscopically determined atmospheric parameters of J005252, HD133656 and SAO239853 obtained using the UVES spectra presented in this study, from Van Winckel et al. (1996a), from Van Winckel (1997), respectively. We note that for the Galactic objects HD133656 and SAO239853, there are no luminosity and $E(B-V)$ measurements available.

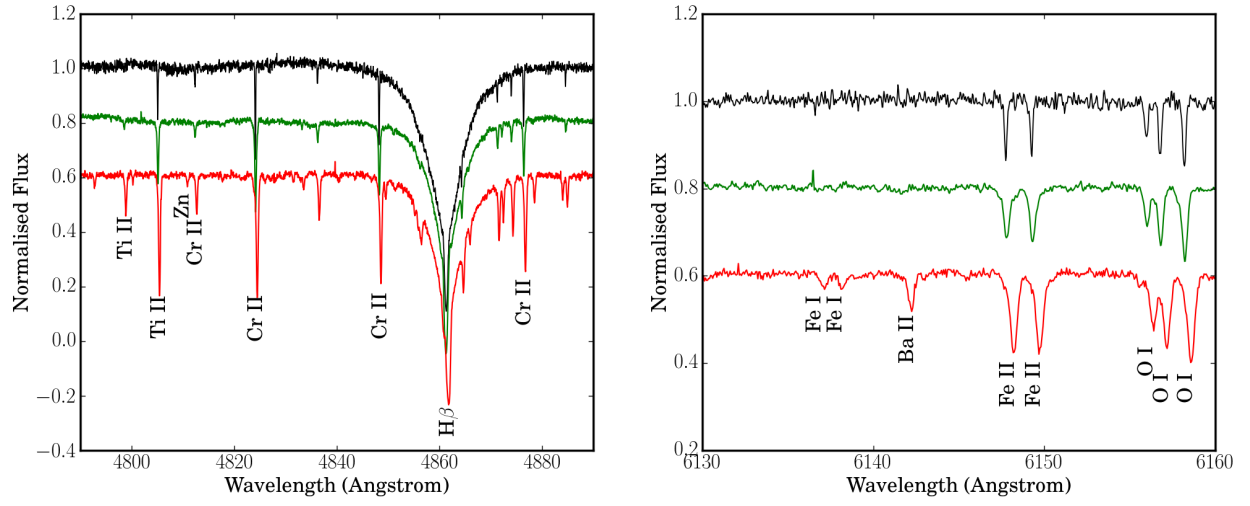


Fig. 12.— Normalised spectral samples of J005252 (in black), HD133656 (in green) and SAO239854 (in red).

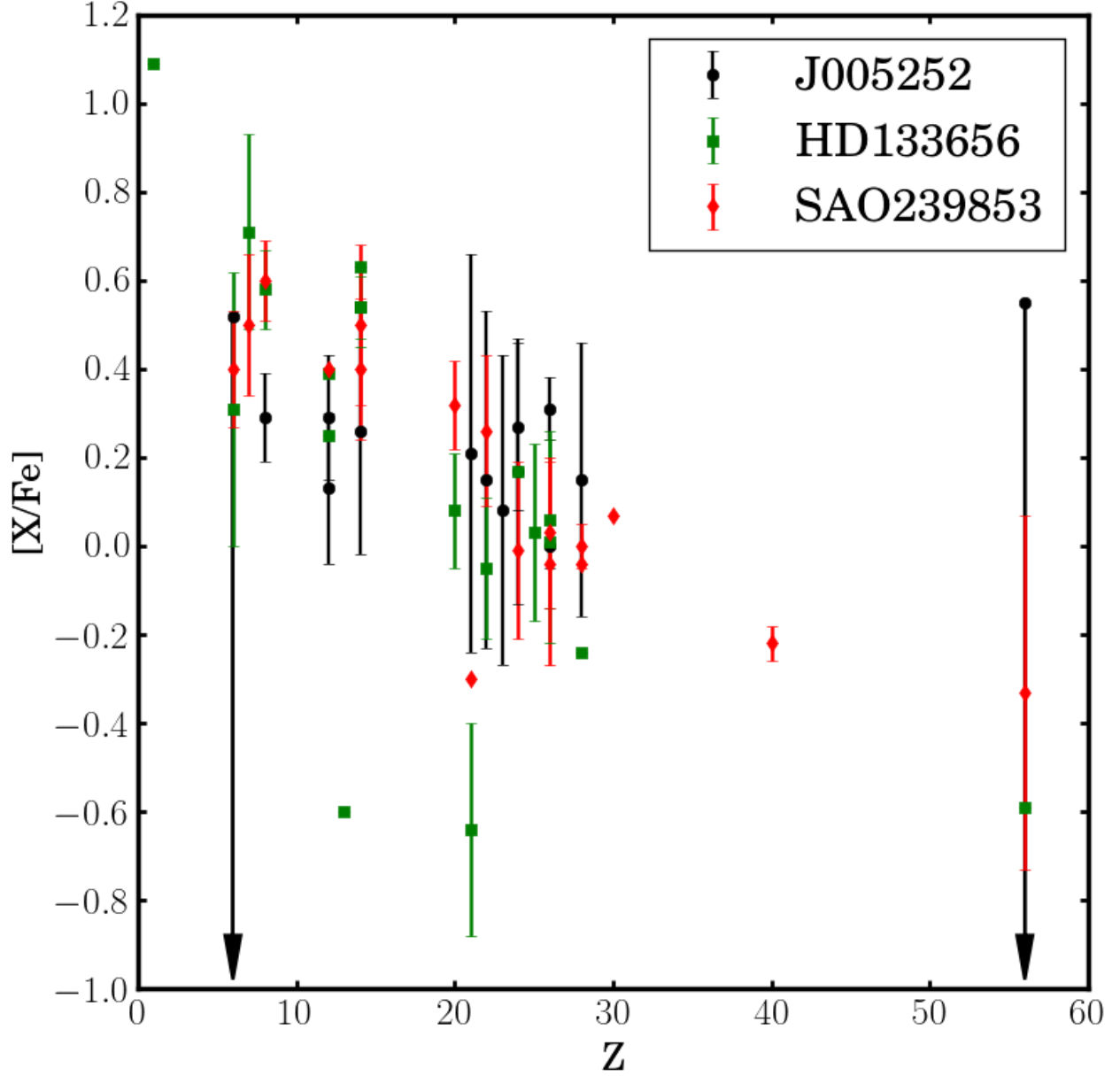


Fig. 13.— Element over hydrogen $[X/Fe]$ ratios of J005252 (in black), HD133656 (in green) and SAO239854 (in red). The error bars represent the total uncertainties σ_{tot} in $[X/Fe]$. Note: For J005252, the abundances of C ($Z=6$) and Ba ($Z=56$) are upper limits and marked with downward arrows. For J005252, the O I and Fe I we plot are the abundances corrected for NLTE effects (see Table 4).